Ocean Engineering 195 (2020) 106733

Contents lists available at ScienceDirect

Ocean Engineering

journal homepage: www.elsevier.com/locate/oceaneng

Numerical modeling of the subaerial landslide source of the 22 December 2018 Anak Krakatoa volcanic tsunami, Indonesia

Mohammad Heidarzadeh [a,*], Takeo Ishibe [b], Osamu Sandanbata [c], Abdul Muhari [d], Antonius B. Wijanarto [e]

[a] Department of Civil & Environmental Engineering, Brunel University London, Uxbridge, UB8 3PH, UK
[b] Association for the Development of Earthquake Prediction, Tokyo, 101-0064, Japan
[c] Earthquake Research Institute, The University of Tokyo, Tokyo, 113-0032, Japan
[d] Ministry of Marine Affairs and Fisheries, Jakarta, 10110, Indonesia
[e] Badan Informasi Geospasial, Cibinong, Indonesia

ARTICLE INFO

Keywords:
Volcanic tsunami
Anak Krakatoa
Sunda Strait
Numerical simulations
Indonesia
Wavelet

ABSTRACT

The eruption of the Anak Krakatoa volcano (Indonesia) in December 2018 produced a destructive tsunami with maximum runup of 13 m killing 437 people. Since the occurrence of this rare tsunami, it has been a challenge as how to model this tsunami and to reconstruct the network of coastal observations. Here, we apply a combination of qualitative physical modeling and wavelet analyses of the tsunami as well as numerical modeling to propose a source model. Physical modeling of a volcano flank collapse showed that the initial tsunami wave mostly involves a pure-elevation wave. We identified initial tsunami period of 6.3–8.9 min through Wavelet analysis, leading to an initial tsunami dimension of 1.8–7.4 km. Twelve source models were numerically modelled with source dimensions of 1.5–4 km and initial tsunami amplitudes of 10–200 m. Based on the qualities of spectral and amplitude fits between observations and simulations, we constrained the tsunami source dimension and initial amplitude in the ranges of 1.5–2.5 km and 100–150 m, respectively. Our best source model involves potential energy of 7.14×10^{13}–1.05×10^{14} J equivalent to an earthquake of magnitude 6.0–6.1. The amplitude of the final source model is consistent with the predictions obtained from published empirical equations.

1. Introduction

A large tsunami reaching a maximum runup height of 13 m (Muhari et al., 2019) was generated in the Sunda Strait, Indonesia due to volcanic activities of the Anak Krakatoa Volcano in the evening of 22 December 2018 (Fig. 1). No large earthquake was reported before the tsunami whereas volcanic activities were observed at the Krakatoa Volcano from a few months earlier until the time of the destructive tsunami of 22 December, according to media reports. Therefore, it is widely believed that the tsunami was generated by volcano-related mass failures and associated subaerial landslides. Satellite images from the Sunda Strait before and after the event revealed that a large portion of the middle Krakatoa volcano island (known as Anak Krakatoa) collapsed into the sea as a result of the volcanic eruption (Fig. 1b). The tsunami left a death toll of at least 437 (https://reliefweb.int) as of 6th January 2018. The Krakatoa volcano tsunami occurred approximately three months after another destructive tsunami in east Indonesia, the 2018 Sulawesi tsunami, claiming around 2000 lives, which was partially attributed to subaerial/submarine landslides (Heidarzadeh et al., 2018; Takagi et al., 2019). The main eruption, responsible for the Anak Krakatoa tsunami, was also recorded at seismic stations in the region (Fig. 2). Based on these seismic records, the origin time of the eruption was approximately at 13:56 UTC on 22 December 2018 (Fig. 2).

Indonesia is home to approximately 130 volcanoes (Lavigne et al., 2008), a number of which are located in the sea and are capable of producing tsunamis. Possibly the predecessor of the December 2018 destructive volcanic tsunami was another deadly volcanic tsunami around the same place in 1883 generated by the Krakatoa eruption with 36000 deaths (Choi et al., 2003; Pelinovsky et al., 2005). Based on Bryant (2001), the 1883 event produced at least 20 Km^3 of pyroclastic deposits. For the 1883 event, tsunami wave runup was approximately 15 m on the average in the near field, i.e. coasts of Sunda Strait, but maximum wave runup was up to 42 m during the 1883 Krakatoa tsunami (Choi et al., 2003). Nomanbhoy and Satake (1995) modelled

* Corresponding author.
E-mail address: mohammad.heidarzadeh@brunel.ac.uk (M. Heidarzadeh).

https://doi.org/10.1016/j.oceaneng.2019.106733
Received 30 June 2019; Received in revised form 24 September 2019; Accepted 11 November 2019
Available online 19 November 2019

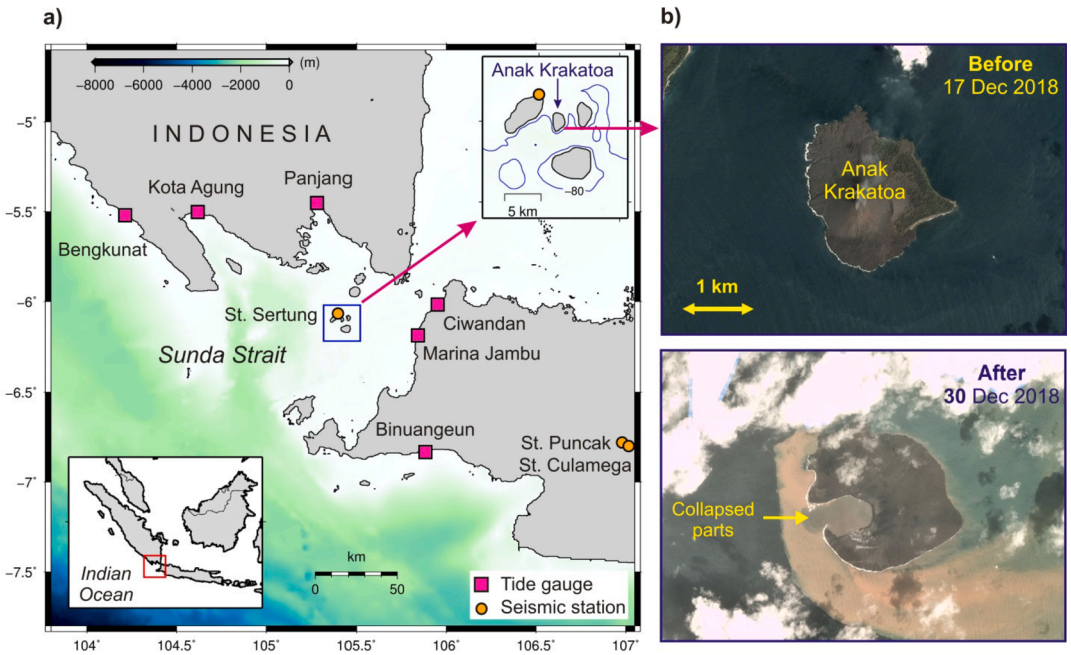

Fig. 1. a): Geographical location of the Sunda Strait and the bathymetry of the region including the Anak Krakatoa volcano. Solid squares and circles are the locations of tide gauges and seismic stations, respectively, which are used in this study. b) Satellite images from the Sunda Strait before and after the event from Planet Labs Inc (www.planet.com).

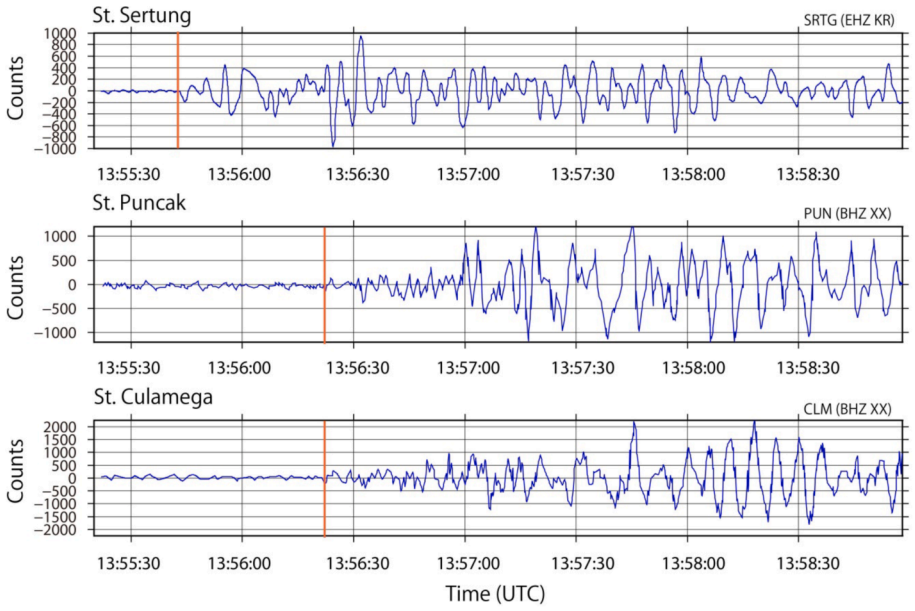

Fig. 2. Seismic records at three seismic stations in the Sunda Strait and Java Island (data from: http://www.vsi.esdm.go.id). Red vertical lines indicate arrival times of the seismic waves associated with the volcanic eruption. All seismic records are vertical components. See Fig. 1 for the locations of these seismic stations. (For interpretation of the references to colour in this figure legend, the reader is referred to the web version of this article.)

the 1883 event using nonlinear shallow water equations and successfully reproduced the 1883 tsunami. Latter (1981) provided a detailed review of the 1883 Krakatoa tsunami including origin time, period and coastal amplitudes of the waves and arrival times.

Tsunamis generated by volcanic activities are generally less understood due to the scarcity of such events. To reproduce the propagation and coastal amplification of volcanic tsunamis, it is essential to estimate the source of these tsunamis. Several authors in the past have studied source mechanism of volcano tsunamis. Latter (1981) listed 10 mechanisms for generation of volcanic tsunamis worldwide among which the most destructive are those generated by the impacts of pyroclastic flow deposits into the sea as well as volcanic-triggered landslides. According to Latter (1981), tsunamis from pyroclastic flows are rare while those generated by volcanic-triggered landslides are more common. Paris et al. (2014) presented a review of volcanic tsunamis including 40 incidents worldwide in the period of 1550–2007 and discussed their generation mechanisms. Eight mechanisms were proposed by Paris et al. (2014): underwater explosion, pyroclastic flow, earthquake, flank failure, caldera subsidence, air wave, lahar and collapse of the lava bench. Caldera uplift associated with volcanic activities can be considered as another generation mechanism for volcanic tsunamis as evidenced during the 2015 Torishima volcanic tsunami, Japan (Sandanbata et al.,

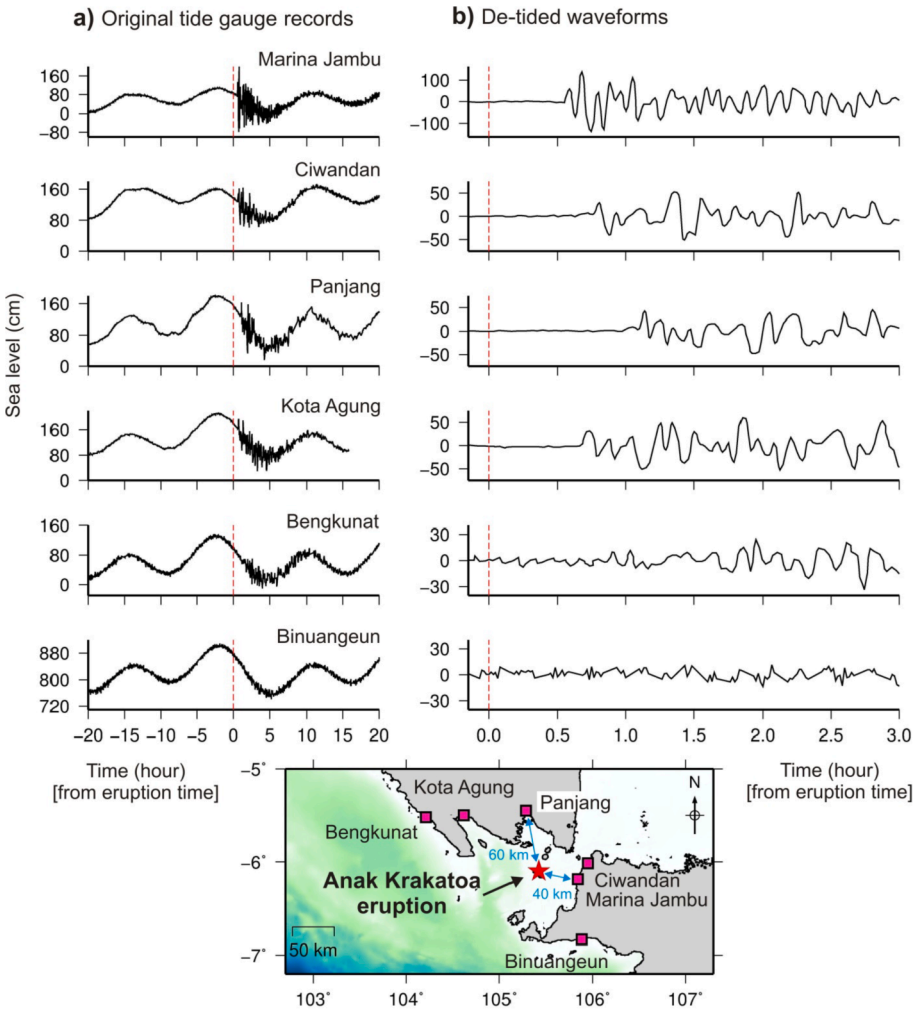

Fig. 3. a): The observed tide gauge records of the 22 December 2018 Anak Krakatoa volcanic tsunami. b): the de-tided records.

2018a; Fukao et al., 2018). The 2002 Stromboli volcanic tsunami was reported by Tinti et al. (2006) who measured a maximum runup of 11 m and associated the tsunami to two landslides with a combined mass volume of 0.02–0.03 km^3. Satake (2007) modelled the 1741 Oshima-Oshima volcanic tsunami in the Japan Sea whose landslide volume was estimated to be approximately 2.5 km^3. A new modeling of the Oshima-Oshima volcanic tsunami was conducted by Ioki et al. (2019) estimating the volume of the collapsed material at 2.2 km^3.

The December 2018 Krakatoa volcanic tsunami is among a few examples of relatively well-recorded volcanic tsunamis worldwide as the tsunami was recorded by several tide gauges. It is, therefore, an important event whose study will contribute to better understanding of coastal hazards from volcanic tsunamis. Here, we study the source of the recent Anak Krakatoa volcanic tsunami using tide gauge data and numerical simulations. We propose a static source model which fairly reproduces the observed tide gauge data.

2. Data and methods

Our approach to estimate the tsunami source model of the December 2018 Anak Krakatoa tsunami was based on: first, determination of the type of the source (either a dipole depression-elevation wave or a pure-elevation wave) using qualitative physical experiment; second, approximation of the source dimensions using Wavelet analysis of the tide gauge records; and third, validation of the source model using forward numerical modeling of the tsunami. Our tsunami numerical modeling is based on assuming an initial tsunami wave at the end of the generation phase and then modeling its propagation and coastal amplification. In fact, we consider a static model and ignore the initial complicated tsunami generation phase. The term "static model" here implies that the complex two-phase flow consisting of water-soil interaction at the beginning of the slide motion (10–100 s) is ignored. This approach has been successfully applied to the 1998 Papua New Guinea landslide tsunami (Synolakis et al., 2002; Okal and Synolakis, 2004; Heidarzadeh and Satake, 2015a), the September 2013 landslide tsunami in the NW Indian Ocean (Heidarzadeh and Satake, 2014) and the 1945 Makran tsunami (Heidarzadeh and Satake, 2017). This forward modeling trial-and-error approach is useful for the case of the Anak Krakatoa tsunami because alternate methods, such as tsunami inversion, may not yield satisfactory results due to the complexity of the source mechanism and lack of high-resolution bathymetry data. For our trial-and-error approach, first we consider a hypothetical source and conduct tsunami propagation and compare the synthetic waveforms with actual tide gauge observations. Wee modify the assumed tsunami source according to the quality of match between synthetic and observed waveforms and continue this process until satisfactory match is achieved.

Sea level data consists of six tide gauge records (see Fig. 1a for locations) with sampling intervals of 1 min provided by the Agency for Geo-spatial Information, Indonesia (BIG) (http://tides.big.go.id). To remove tidal signals from the original records, we predicted the tidal signals using a least squares method of harmonic analysis and then removed them from the original records (Fig. 3). Wavelet, time–frequency, analysis was performed by applying the Wavelet package of

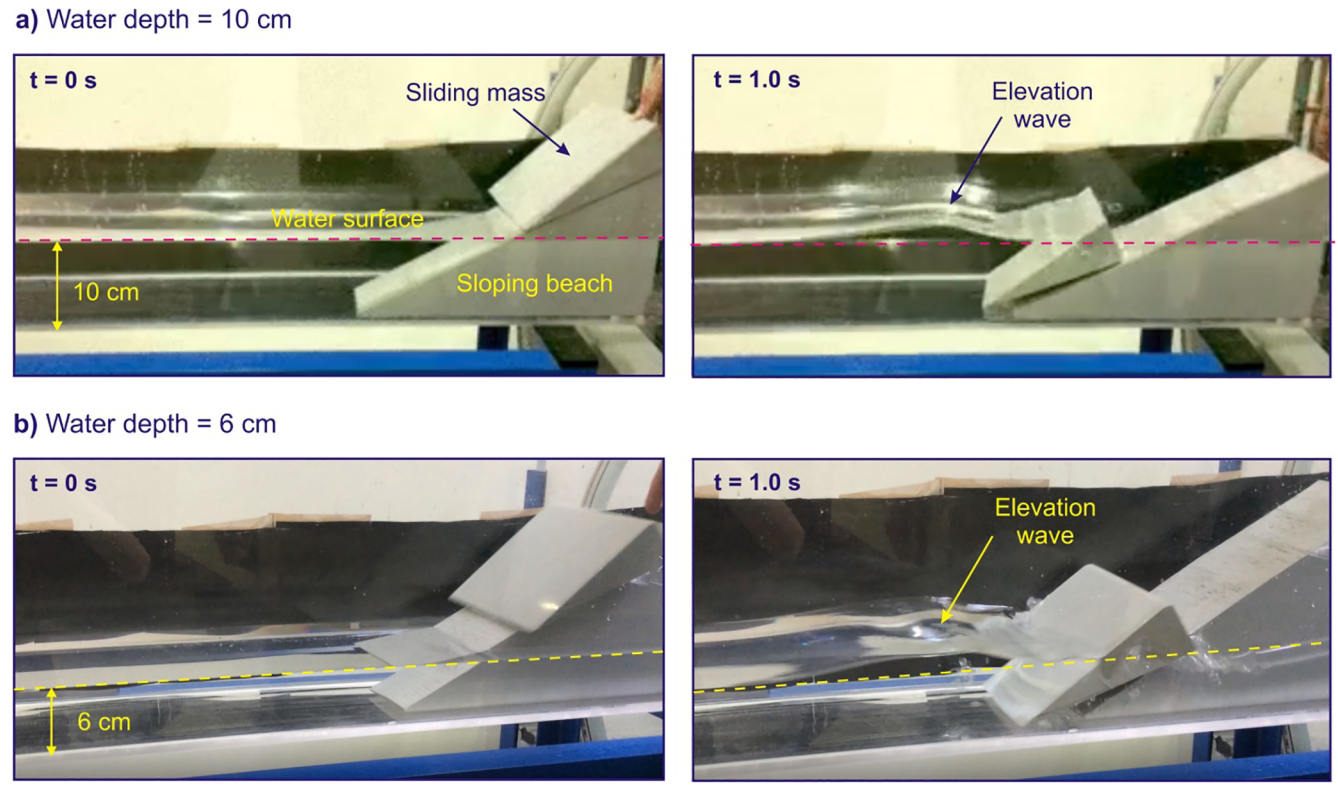

Fig. 4. Qualitative physical experiments on the initial waves generated by the flank collapse of a volcano at two water depths of 10 cm (a) and 6 cm (b). This experiment is similar to the volcano flank collapse which occurred during the 22 December 2018 Anak Krakatoa eruption.

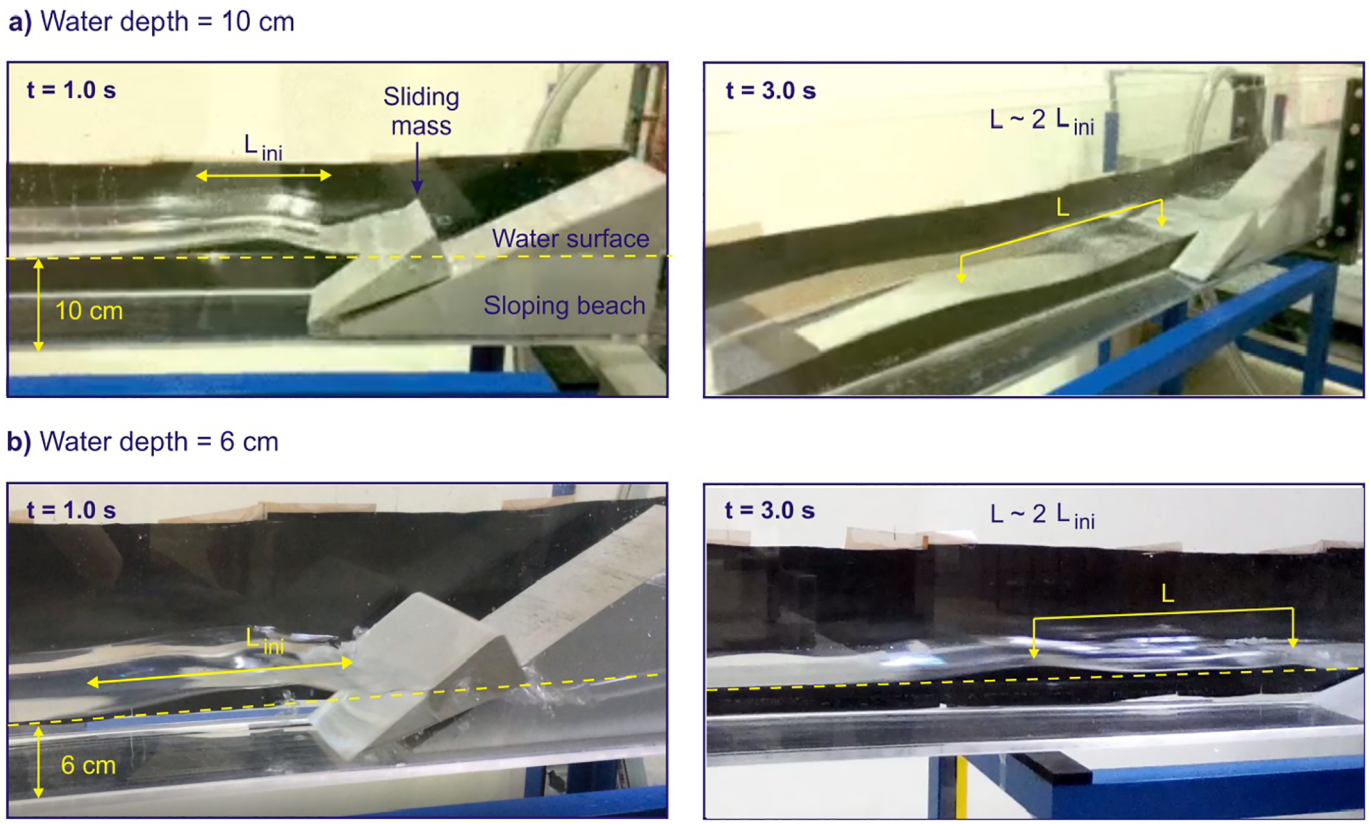

Fig. 5. Qualitative physical experiments on the relationship between initial source length (L_{ini}) and tsunami wavelength (L) for two cases of volcano flank collapses at water depths of 10 cm (a) and 6 cm (b).

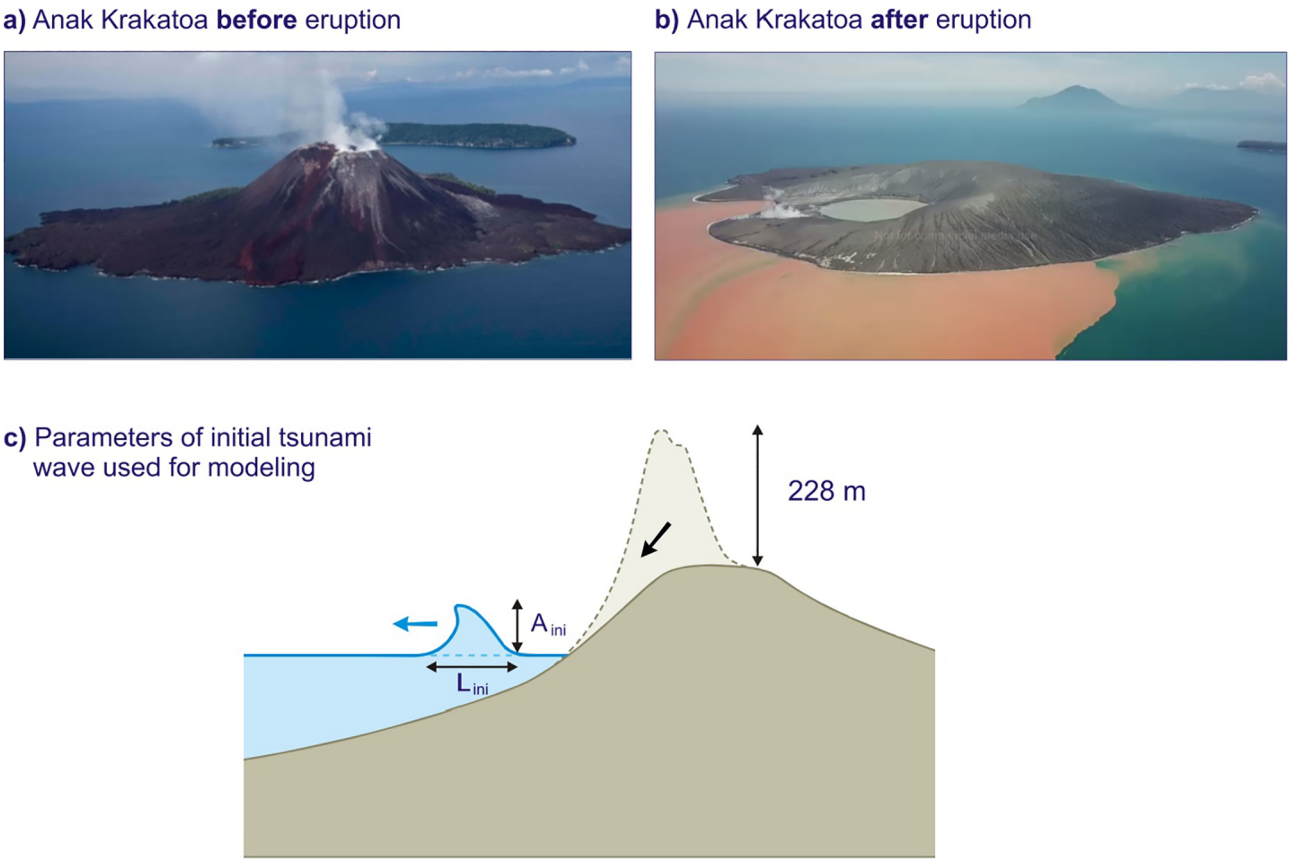

Fig. 6. Photographs and sketch showing the Anak Krakatoa volcano before and after the 22 December 2018 eruption. Photos shown in panels "a" and "b" are from https://www.jp-news.id/v/2651/dua-kali-letusan-setinggi-300-meter-tingkat-aktivitas-gunung-anak-krakatau-berstatus-waspada and www.youtube.com/watch?v=I-3A4GR-VnU, respectively. The data of height difference for before and after the eruption is from https://sp.hazardlab.jp/know/topics/detail/2/7/27793.html. This is a Japanese website informing that the height of the mountain dropped from 338 m to 110 m. A_{ini} and L_{ini} are initial wave amplitude and initial length of the tsunami source, respectively.

Torrence and Compo (1998). Our Wavelet analysis was conducted using the Morlet mother function with a wavenumber of 6 and a scale width of 0.10 (Heidarzadeh et al., 2015).

The COMCOT numerical package (Cornell Multi-grid Coupled Tsunami Model), which is based on nonlinear Shallow Water equations (Liu et al., 1998; Wang and Liu, 2006), was applied for tsunami simulations. A uniform bathymetry grid with a resolution of 8 arc-sec (approximately 250 m) was used. The bathymetry grid was interpolated from the GEBCO-2014 (The General Bathymetric Chart of the Oceans) 30 arc-sec bathymetric digital atlas (Weatherall et al., 2015). We excluded runup calculations in our numerical simulations because it requires high-resolution nearshore bathymetry/topography. Nonlinear simulations were conducted for a total time of 3 h with a time step of 0.5 s.

3. Type of the initial tsunami source and its dimensions

The type of the initial wave generated by volcanic tsunamis is not well understood in the existing literature. This is the reason that we had to conduct physical experiments to identify the type of the initial wave. Qualitative physical modeling was performed at the wave flume of the Earthquake Research Institute, The University of Tokyo (Japan) (Figs. 4–5) to identify the type of the initial tsunami wave. This was aimed at understanding the general physics of the initial tsunami wave immediately after the generation phase rather than quantitative measurements. Froude similarity is used for physical modeling of coastal problems (Fritz et al., 2004; Sorensen, 2010); however, we do not measure wave parameters in this study because this is a qualitative assessment. The flume has dimensions of 2.6 m (length) × 0.1 m (width) × 0.3 m (height) (Sandanbata et al., 2018b). Numerous subaerial slides were made and the resulting initial waves were photographed (Figs. 4–5). For submarine landslides, it was previously shown by numerous authors that the initial wave has a dipole depression-elevation shape (Synolakis, 2003; Okal and Synolakis, 2004; Okal et al., 2009; Watts et al., 2005; Enet and Grilli, 2007; McFall and Fritz, 2016). However, for the subaerial mass movements, including the flank collapse of a volcano, our experiments revealed that the initial wave is of almost pure elevation shape (Fig. 4). We conducted several experiments using the set-up shown in Figs. 4–5 by varying water depth; all of them showed initial pure-elevation wave. Two examples of our experiments are shown in Fig. 4 at two water depths of 6 and 10 cm. This was previously partially shown by Fritz et al. (2001) for the Lituya Bay subaerial slide experiments. Therefore, we consider an elevation wave as the initial wave for modeling the Anak Krakatoa Volcano tsunami. In comparison to other studies, Walder et al. (2003) also considered a wave hump (i.e. an elevation wave) to model tsunamis from subaerial landslides.

The initial estimation of the tsunami source dimension can be achieved using the equation for phase velocity of long oceanic waves (e.g. tsunamis) (Rabinovich et al., 2006; Rabinovich, 2010; Sorensen, 2010):

$$C = L/T \quad (1)$$

in which, C is tsunami phase velocity, L is tsunami wavelength, and T is the tsunami dominating period. For long waves such as tsunamis, we know that: $C = \sqrt{gh}$ where g is gravitational acceleration (9.81 m/s^2) and h is water depth (Sorensen, 2010). The tsunami wavelength (L) is α

Table 1
Parameters of different pure-elevation waves used for modeling initial sea level disturbance scenarios in this study.

Landslide Scenario (LS)	Location (°E), (°S)	A_{ini} [a] (m)	L_{ini} [b] (km)	V_{ini} [c] (km^3)	Potential energy (J)	Earthquake Magnitude (M)
LS-1	105.4079, −6.1042	50.0	3.0	0.225	3.78×10^{13}	5.9
LS-2	105.4079, −6.1042	100.0	3.0	0.448	1.51×10^{14}	6.3
LS-3	105.4079, −6.1042	150.0	3.0	0.673	3.39×10^{14}	6.5
LS-4	105.4079, −6.1042	150.0	2.0	0.314	1.43×10^{14}	6.2
LS-5	105.4147, −6.1167	88.0	4.0	0.663	2.00×10^{14}	6.3
LS-6	105.4079, −6.1100	88.0	4.0	0.677	2.07×10^{14}	6.3
LS-7	105.4079, −6.1042	150.0	1.5	0.175	7.14×10^{13}	6.0
LS-8	105.4079, −6.1042	200.0	1.5	0.236	1.28×10^{14}	6.2
LS-9	105.4079, −6.1042	100.0	2.5	0.326	1.05×10^{14}	6.1
LS-10	105.4079, −6.1042	150.0	2.5	0.489	2.37×10^{14}	6.4
LS-11	105.4079, −6.1042	10.0	1.0	0.0053	1.09×10^{11}	4.2
LS-12	105.4079, −6.1042	20.0	2.0	0.0417	2.54×10^{12}	5.1

[a] Initial wave amplitude (m) (Fig. 6).
[b] Initial length of the source (km) (Fig. 6).
[c] Volume of the displaced water (km^3).

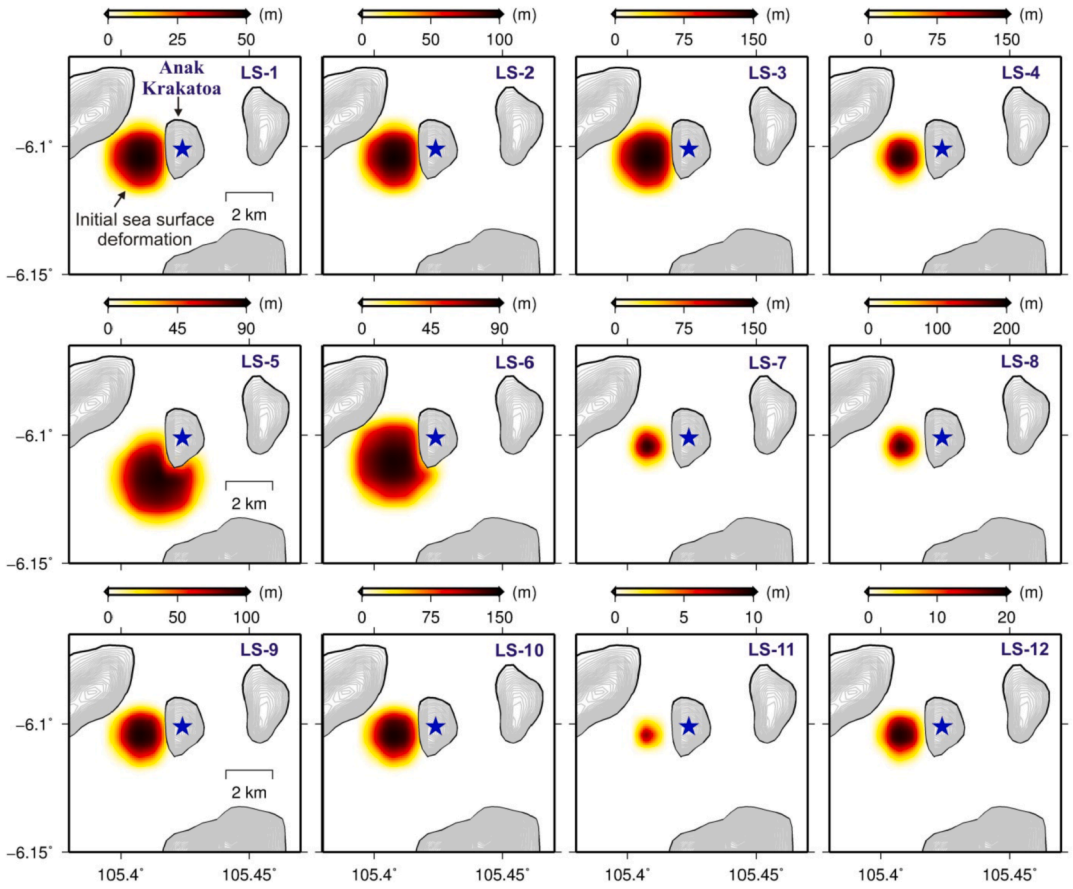

Fig. 7. Different subaerial landslide source scenarios (LS) considered in this study as potential sources of the 22 December 2018 Anak Krakatoa volcanic tsunami. The blue star shows the Anak Krakatoa volcano. (For interpretation of the references to colour in this figure legend, the reader is referred to the web version of this article.)

times larger than the initial length of the source (L_{ini}) around the source region:

$$L = \alpha\, L_{ini} \tag{2}$$

Previously Heidarzadeh and Satake (2015b) reported $\alpha = 2$ which is confirmed by our qualitative physical experiments (Fig. 5). Therefore by combining Equations (1) and (2), we have:

$$L_{ini} = \frac{T}{2}\sqrt{gh} \tag{3}$$

The sketch in Fig. 6c demonstrates the elevations of the Anak Krakatoa volcano before and after the December 2018 eruption and the initial pure-elevation wave considered in this study for modeling the propagation and coastal amplification of the tsunami. The volcano lost 228 m of its top structure to the sea due to the eruption (Fig. 6a,b,c). We consider two parameters for our static initial source model: the initial length of the source (L_{ini}) and the initial wave amplitude (A_{ini}). Twelve different scenarios were considered with varying values of L_{ini} (1.5–4 km) and A_{ini} (10–200 m) (Table 1) inspired by our Wavelet analyses (Section 4). A circular elevation wave is used for the shape of the initial wave (Fig. 7). For each scenario, the potential energy of the initial tsunami source is calculated using the following equation (modified

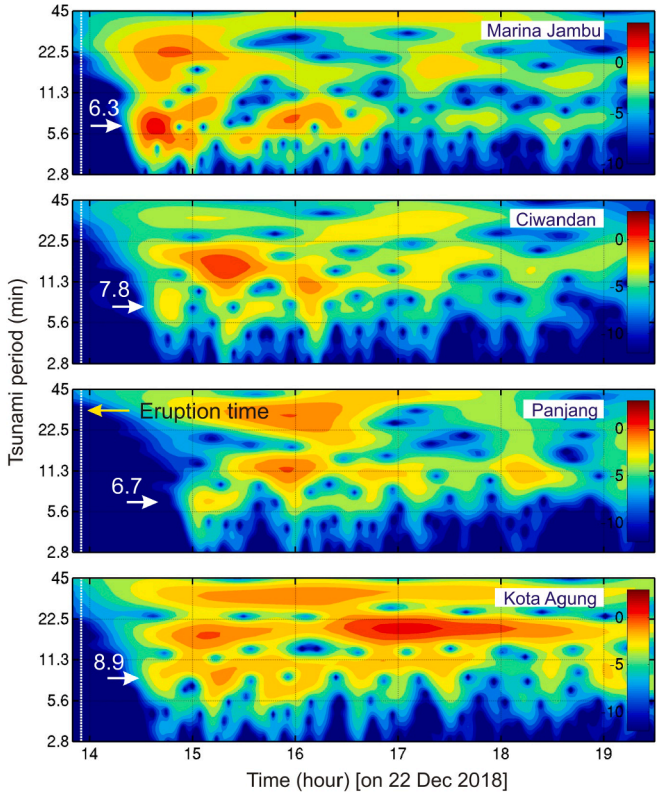

Fig. 8. Wavelet analysis for the tide gauge records of the December 2018 Anak Krakatoa volcanic tsunami. The vertical white dashed line is the time of the tsunamigenic volcanic eruption (i.e. 13:56 UTC).

from Satake and Kanamori, 1991):

$$E_p = \frac{1}{2}\rho g \sum_{i=1}^{n} \eta_i^2 S_i \quad (4)$$

in which, E_p is the potential energy of tsunami initial source in Joules, ρ is density of water which is assumed to be 1000 kg/m^3, g is gravitational acceleration (9.81 m/s^2), i is a counter for the number of computational cells, n is the total number of cells in the computational domain, η_i is the amplitude of the initial tsunami source scenario at the center of each cell, and S_i is the area of each computational cell (S_i= 250 m × 250 m = 62500 m^2). To convert the potential energy of tsunami (E_p, Joules) to an equivalent earthquake magnitude (in Richter scale), the Gutenberg-Richter equation was used (Gutenberg and Richter, 1956):

$$\log E = 4.8 + 1.5\, M_s \quad (5)$$

in which, E is energy released by the earthquake in Joules, *log* is the logarithm to the base 10 and M_s is earthquake surface-wave magnitude. We used E_p of each source scenario as inputs for E in Equation (5). Both amplitudes and spectra of the simulated waveforms were compared with those of observations at tide gauges in order to select the best source model. For amplitude comparisons, the Normalized Root Mean Square (NRMS) misfit equation of Heidarzadeh et al. (2016a) was applied.

As subaerial landslide-generated waves are usually characterized by short-period waves, it is necessary to quantify the degree of wave dispersion in order to confirm whether Shallow Water equations used by COMCOT are adequate for their simulations. We apply the following wave dispersion parameter introduced by Glimsdal et al., (2013):

$$\tau = \frac{6h^2 d}{\lambda^3} \quad (6)$$

in which τ is dispersion parameter, λ is length of tsunami source, h is water depth around the source region, and d is the distance from source region to the coastline. Dispersion effect can be neglected for $\tau < 0.01$ but it becomes significant if $\tau > 0.1$ (Glimsdal et al., 2013). For the case of the 22 December 2018 Anak Krakatoa volcanic tsunami, we have: $\lambda = 1.5$–4 km (Table 1), $d = 40$–80 km (Fig. 3) and $h = 0$–100 m (Fig. 1). Therefore, we obtain an average value of 0.04 for the dispersion parameter (τ) implying that dispersion effects is not significant.

4. Source dimensions based on wavelet analysis

Fig. 8 presents the results of Wavelet analysis which reveals that tsunami energy is distributed in the period band of 5–25 min. It can be seen that energy is channeled into varying period bands at different times. For example, three period bands of 6.3, 17 and 23 min are identified in the Wavelet plot of Marina Jambu. The high-energy channels for Kota Agung are 8.9 and 17 min. Different tsunami dominating periods are seen from one station to another. In Marina Jambu the dominating period is 6.3 min while it is 15 min in Ciwandan, 11.4 min in Panjang and 17 min in Kota Agung. Appearance of several high-energy channels and occurrence of different dominating periods can be attributed to the complicated bathymetry features in the Sunda Strait which includes shallow water (<1000 m water depth) and several small islands and coastal rias (Fig. 1). Therefore, not all of the high-energy tsunami periods can be attributed to the tsunamis source itself (e.g., Rabinovich, 1997; Heidarzadeh et al., 2016b). It has been reported by several authors that the first tsunami waves can be considered as those generated by the tsunami source (e.g., Rabinovich, 2010; Rabinovich et al., 2008; Heidarzadeh and Satake, 2013). The Wavelet analysis shows that the period of the first tsunami waves are 6.3, 7.8, 6.7 and 8.9 min in the four tide gauge stations, indicating that the average source period of the December 2018 Anak Krakatoa tsunami was 7.4 min which is the mean value of the aforesaid four periods. Applying Equation (3), by considering water depth in the range of 10–80 m and wave period of 6.3–8.9 min, we estimate the initial water surface dimension (L_{ini}) in the range of 1.8–7.4 km. Our source scenarios (Table 1, Fig. 7) include initial source lengths (L_{ini}) in the range of 1.5–4.0 km because preliminary simulations revealed that source lengths larger than 4.0 Km result is synthetic waveforms much larger than observations.

5. Best source model based on numerical simulations and discussion

Simulated waveforms for 12 subaerial landslide scenarios (LS) are compared with observed waveforms (Fig. 9). Results showed that scenarios with initial wave amplitude (A_{ini}) of 10–20 m (LS-11 & LS-12) cannot generate any waves at the location of five tide gauges. On the other hand, scenarios involving large initial length (L_{ini}) of 4.0 km (LS-5 & LS-6) generate much larger simulated waves than observations. In terms of quality of amplitude fit between observations and simulations, five scenarios (LS-1, LS-4, LS-7, LS-8, and LS-9) produce better performances (Figs. 9–10). These five scenarios cover initial lengths and amplitudes in the ranges of 1.5–3 km and 50–200 m, respectively. The minimum NRMS misfit belongs to LS-7 (Fig. 10).

To further narrow down our search for the best source model, we calculated the water wave spectra for the five scenarios of LS-1, LS-4, LS-7, LS-8, and LS-9 (Fig. 11). It can be seen that the spectra for the observations and simulations match fairly well in Marina Jambu and Panjang. For the two stations of Kota Agung and Ciwandan, the spectral peaks are identical (Fig. 11) although spectral gaps exist between simulations and observations. Overall, LS-9 better reproduces the observation spectra than the other scenarios.

In summary, the best model in terms of amplitude fit between observations and simulation is LS-7 whereas it is LS-9 in terms of spectral fit. Considering the uncertainties involved in this research such as lack of

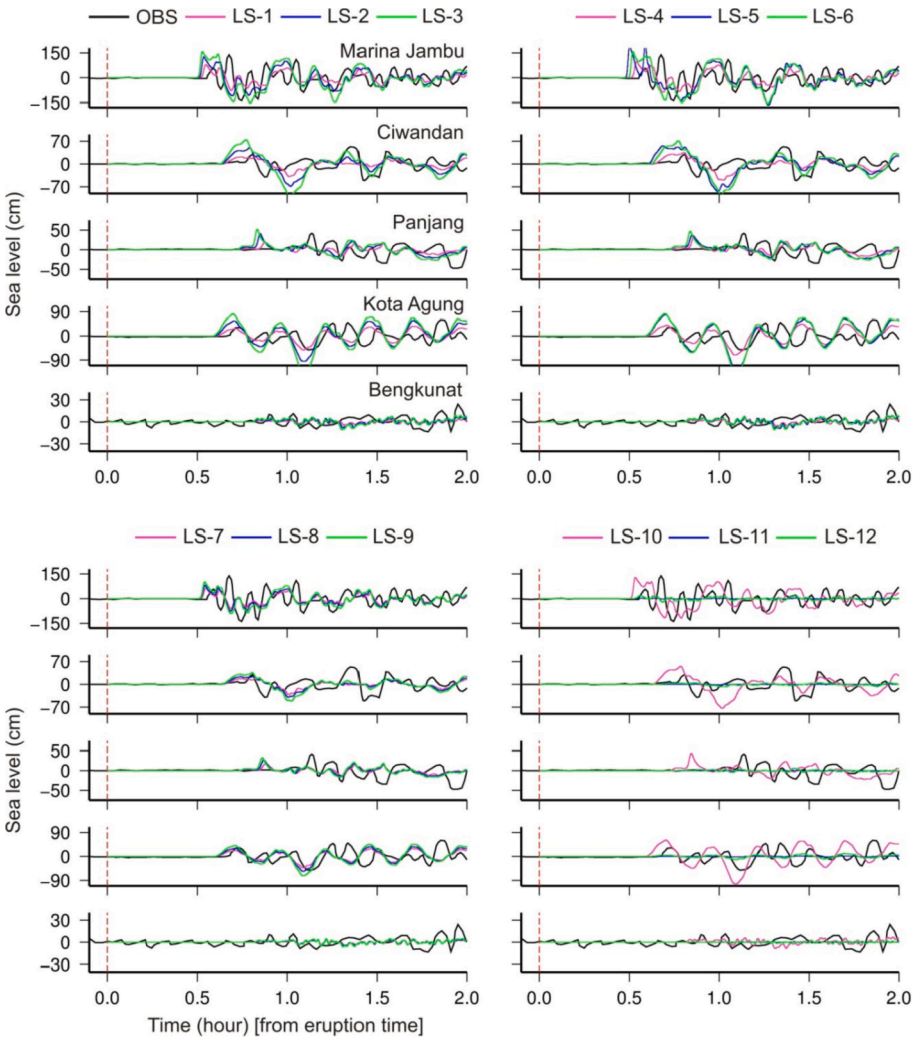

Fig. 9. Comparison of observed (black) and simulated (colored) tsunami waveforms from various scenarios for the December 2018 Anak Krakatoa volcanic tsunami. The vertical dashed line is the time of the tsunamigenic volcanic eruption (i.e. 13:56 UTC). (For interpretation of the references to colour in this figure legend, the reader is referred to the web version of this article.)

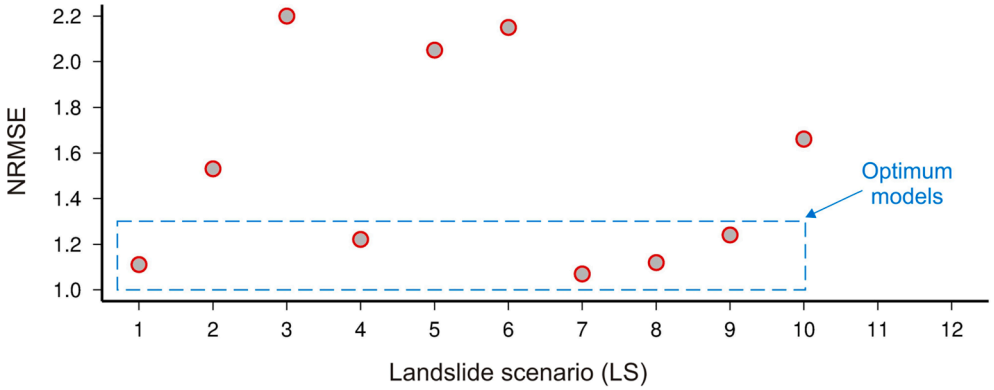

Fig. 10. NRMSE (Normalized Root Mean Square Error) for various source models for the 22 December 2018 Anak Krakatoa volcanic tsunami. The blue dashed rectangle shows the optimum models. (For interpretation of the references to colour in this figure legend, the reader is referred to the web version of this article.)

high-resolution bathymetry, limited tide gauge data available, and the limited number of tsunami scenarios used, it is believed that a single source model should not be chosen as the best model. Rather, the best model could have characteristics between LS-7 and LS-9 (Fig. 12). Therefore, we report the initial length and initial wave amplitude of the best model in the ranges of L_{ini} = 1.5–2.5 km, and A_{ini} = 100–150 m, respectively. Such a source model produces potential energy of 7.14×10^{13}–1.05×10^{14} J equivalent to an earthquake of magnitude 6.0–6.1 (in Richter scale) (Table 1).

Our final source model (L_{ini} = 1.5–2.5 km; A_{ini} = 100–150 m) is consistent with published empirical equations on the maximum amplitude of the initial wave generated by subaerial landslides (Table 2) (Fritz

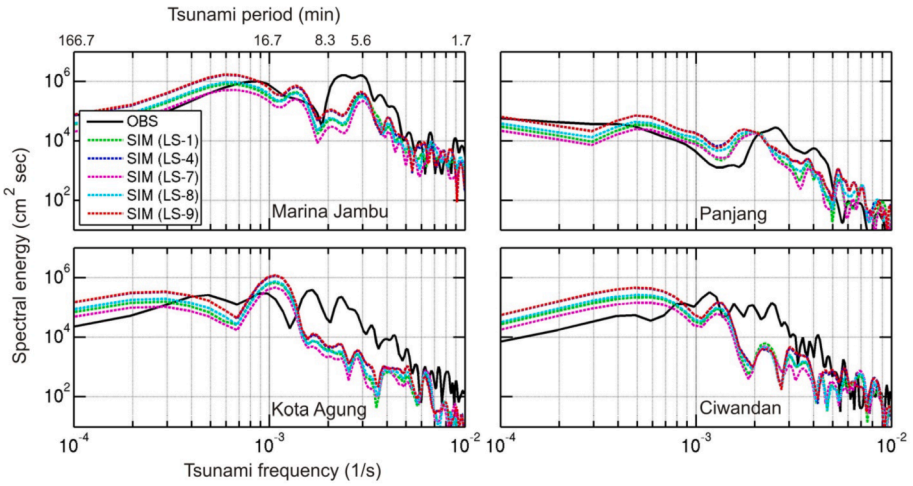

Fig. 11. Comparison of observed (black) and simulated (colored) tsunami spectra for the optimum models (LS-1, 4, 7, 8 and 9) of the December 2018 Anak Krakatoa volcanic tsunami. (For interpretation of the references to colour in this figure legend, the reader is referred to the web version of this article.)

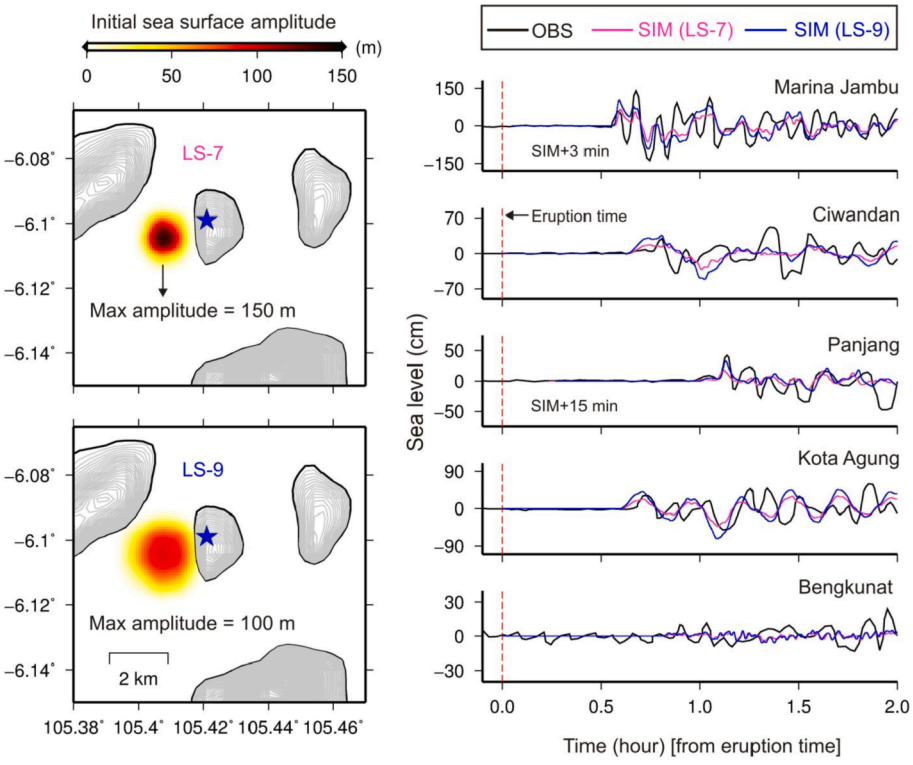

Fig. 12. Two final source models for the December 2018 Anak Krakatoa volcanic tsunami.

et al., 2004, 2009; Noda, 1970). By using the characteristics of the December 2018 Anak Krakatoa volcanic eruption, such as average slide thickness (s) of 114 (half of the total collapsed height of 228 m, Fig. 6), average water depth (h) of 20–50 m, friction factor (f) of 0.1, slide impact angle (α) of 45°, rock density of 2300 kg/m^3, water density of 1000 kg/m^3, slide volume (V_s) of 21.1×10^6 m^3(volume of a cone with height of 228 m and radius of 300 m; Figs. 1 and 6), the empirical equations yield initial wave amplitude (A_{ini}) of 65–134 m (Table 2) which is fairly close to our A_{ini} = 100–150 m. The final initial source dimension of L_{ini} = 1.5–2.5 km is within the estimated range of source length from wavelet analysis (L_{ini} = 1.8–7.4 km). We note that the existing empirical equations for the prediction of the maximum amplitude of the initial wave generated by subaerial landslides are associated with large uncertainties as seen in the amplitude range of 65–134 m given by these equations (Table 2).

6. Conclusions

The 22 December 2018 tsunami generated by the eruption of the Anak Krakatoa volcano has been studied and a source model is proposed. Main findings are:

- Our qualitative physical modeling of subaerial landslide failures revealed that the initial tsunami wave, immediately after the generation phase, is mostly a pure-elevation wave. Therefore, the tsunami source was assumed to be a pure-elevation wave in this study.

Table 2
Comparison of initial wave amplitudes for the December 2018 Anak Krakatoa volcanic tsunami obtained from our numerical experiments with those of predictive equations.

Reference	Predictive equation[a]	A_{ini}[b] (m)
This study	Numerical modeling	100–150
Fritz et al. (2004)	$a_c = 0.25\left(\frac{v_s}{\sqrt{gh}}\right)^{1.4}\left(\frac{s}{h}\right)^{0.8}$	65–103
Noda (1970)	$\frac{a_c}{h} = 1.32\left(\frac{v_s}{\sqrt{gh}}\right)$	85–134

[a] In these equations, the parameters are: a_c is the maximum positive wave amplitude which is equivalent to A_{ini} in this study, h is mean sea water depth (20–50 m), v_s is slide centroid velocity at impact [using the equation $v_s = \sqrt{2g\,\Delta z\,(1 - fcot\alpha)}$ in which Δz is slide centroid drop height, f is friction coefficient (0.1), α is slide impact angle (45°)], s is slide thickness (112 m), ρ_s is density of slide material (2300 kg/m^3), ρ_w is water density (1000 kg/m^3), and V_s is slide volume (21.1×10^6 m^3). The slide centroid velocity at impact is estimated at: $v_s = 44.9\,m/s$.

[b] Initial tsunami wave amplitude (m) (Fig. 6).

- Based on the wavelet analyses of the tsunami observations at tide gauges, we found the period of the first tsunami signal arriving at different stations in the range of 6.3–8.9 min which guided us to an initial tsunami length of 1.8–7.4 km.
- We considered 12 source scenarios, each including a pure-elevation wave, involving source dimensions of 1.5–4 km and initial amplitudes of 10–200 m. Numerical modeling of tsunami was conducted for all 12 source scenarios resulting in five scenarios as the best ones in terms of quality of waveform fits between observations and simulations. These five scenarios narrowed down the source lengths and initial amplitudes to the domains 1.5–3.0 km, and 50–200 m, respectively. Quality of spectral fit between observations and simulations further constrained the source to two models having initial lengths and amplitudes of 1.5–2.5 km and 100–150 m, respectively.
- The best model (length = 1.5–2.5 km; amplitude = 100–150 m) involves potential energy of 7.14×10^{13}–1.05×10^{14} J equivalent to an earthquake of magnitude 6.0–6.1 (in Richter scale). The amplitude of our final model (100–150 m) is consistent with predictions of empirical equations which give initial amplitudes of 65–134 m for the Anak Krakatoa volcano eruption.

Acknowledgements

Agency for Geo-spatial Information (BIG), Indonesia (http://tides.big.go.id) supplied the tide gauge records used in this study. We sincerely thank scientists in BIG including Andi Eka Sakya, Hasanuddin Z Abidin and Mohamaad Arief Syafi'i for their efforts to provide the data in a timely manner. We are grateful to HyeJeong Kim, Taku Ueda, Naoto Yokotani (all from University of Tokyo, Japan) for helping us to perform the physical modeling part of this study. The GMT mapping tool by Wessel and Smith (1998) were used to draft figures. The article benefited from constructive review comments from two anonymous reviewers. MH was funded by the Royal Society grant number CHL\R1\180173 and the Great Britain Sasakawa Foundation grant number 5542 (2018/19).

References

Bryant, T., 2001. Tsunamis, the Underrated Hazard. Cambridge University Press, p. 320. ISBN 0-521-77599-X.
Choi, B.H., Pelinovsky, E., Kim, K.O., Lee, J.S., 2003. Simulation of the trans-oceanic tsunami propagation due to the 1883 Krakatau volcanic eruption. Nat. Hazards Earth Syst. Sci. 3 (5), 321–332.
Enet, F., Grilli, S.T., 2007. Experimental study of tsunami generation by three-dimensional rigid underwater landslides. J. Waterw. Port, Coast. Ocean Eng. 133 (6), 442–454.
Fritz, H.M., Hager, W.H., Minor, H.E., 2004. Near field characteristics of landslide generated impulse waves. J. Waterw. Port, Coast. Ocean Eng. 130, 287–302.
Fritz, H.M., Hager, W.H., Minor, H.-E., 2001. Lituya Bay case rockslide impact and wave run-up. Sci. Tsunami Hazards 19 (1), 3–22.
Fritz, H.M., Mohammed, F., Yoo, J., 2009. Lituya Bay landslide impact generated mega-tsunami 50th anniversary. Pure Appl. Geophys. 166, 153–175.
Fukao, Y., Sandanbata, O., Sugioka, H., Ito, A., Shiobara, H., Watada, S., Satake, K., 2018. Mechanism of the 2015 volcanic tsunami earthquake near Torishima, Japan. Sci. Adv. 4 (4), eaao0219.
Glimsdal, S., Pedersen, G.K., Harbitz, C.B., Løvholt, F., 2013. Dispersion of tsunamis: does it really matter? Nat. Hazards Earth Syst. Sci. 13, 1507–1526.
Gutenberg, B., Richter, C.F., 1956. Magnitude and energy of earthquakes. Ann. Geofisc. 9, 1–15.
Heidarzadeh, M., Satake, K., 2013. The 21 may 2003 tsunami in the Western Mediterranean sea: statistical and wavelet analyses. Pure Appl. Geophys. 170 (9), 1449–1462.
Heidarzadeh, M., Satake, K., 2014. Possible sources of the tsunami observed in the northwestern Indian Ocean following the 2013 September 24 Mw 7.7 Pakistan inland earthquake. Geophys. J. Int. 199 (2), 752–766.
Heidarzadeh, M., Satake, K., 2015. Source properties of the 1998 July 17 Papua New Guinea tsunami based on tide gauge records. Geophys. J. Int. 202 (1), 361–369.
Heidarzadeh, M., Satake, K., 2015. New insights into the source of the Makran tsunami of 27 November 1945 from tsunami waveforms and coastal deformation data. Pure Appl. Geophys. 172 (3), 621–640.
Heidarzadeh, M., Satake, K., Murotani, S., Gusman, A.R., Watada, S., 2015. Deep-water characteristics of the trans-pacific tsunami from the 1 April 2014 M w 8.2 Iquique, Chile earthquake. Pure Appl. Geophys. 172 (3), 719–730.
Heidarzadeh, M., Murotani, S., Satake, K., Ishibe, T., Gusman, A.R., 2016. Source model of the 16 September 2015 Illapel, Chile Mw 8.4 earthquake based on teleseismic and tsunami data. Geophys. Res. Lett. 43 (2), 643–650.
Heidarzadeh, M., Harada, T., Satake, K., Ishibe, T., Gusman, A., 2016. Comparative study of two tsunamigenic earthquakes in the Solomon Islands: 2015 Mw 7.0 normal-fault and 2013 Santa Cruz Mw 8.0 megathrust earthquakes. Geophys. Res. Lett. 43 (9), 4340–4349.
Heidarzadeh, M., Satake, K., 2017. A combined earthquake-landslide source model for the tsunami from the 27 November 1945 M 8.1 Makran earthquake. Bull. Seismol. Soc. Am. 107 (2), 1033–1040.
Heidarzadeh, M., Muhari, A., Wijanarto, A.B., 2018. Insights on the source of the 28 September 2018 Sulawesi tsunami, Indonesia based on spectral analyses and numerical simulations. Pure Appl. Geophys. 176, 25–43.
Ioki, K., Tanioka, Y., Yanagisawa, H., Kawakami, G., 2019. Numerical simulation of the landslide and tsunami due to the 1741 Oshima-Oshima eruption in Hokkaido, Japan. J. Geophys. Res. 124 (2), 1991–2002.
Lavigne, F., De Coster, B., Juvin, N., Flohic, F., Gaillard, J.C., Texier, P., Morin, J., Sartohadi, J., 2008. People's behaviour in the face of volcanic hazards: perspectives from Javanese communities, Indonesia. J. Volcanol. Geotherm. Res. 172 (3–4), 273–287.
Latter, J.H., 1981. Tsunamis of volcanic origin: summary of causes, with particular reference to Krakatoa, 1883. Bull. Volcanol. 44 (3), 467–490.
Liu, P.L.-F., Woo, S.-B., Cho, Y.-S., 1998. Computer Programs for Tsunami Propagation and Inundation. Cornell University, Ithaca, N.Y. Technical Report.
McFall, B.C., Fritz, H.M., 2016. Physical modelling of tsunamis generated by three-dimensional deformable granular landslides on planar and conical island slopes. Proc. R. Soc. Lond. A 472, 20160052 (2188).
Muhari, A., Heidarzadeh, M., Nugroho, H.D., Kriswati, E., Supartoyo, Wijanarto, A.B., Afriyanto, B., Imamura, F., Arikawa, T., 2019. The December 2018 Anak Krakatau volcano tsunami as inferred from post-tsunami field surveys and spectral analysis. Pure Appl. Geophys. https://doi.org/10.1007/s00024-019-02358-2 (in revision).
Noda, E., 1970. Water waves generated by landslides. J. Water-w. Harbors Coastal Eng. Div. ASCE 96 (4), 835–855.
Nomanbhoy, N., Satake, K., 1995. Generation mechanism of tsunamis from the 1883 Krakatau eruption. Geophys. Res. Lett. 22 (4), 509–512.
Okal, E.A., Synolakis, C.E., Uslu, B., Kalligeris, N., Voukouvalas, E., 2009. The 1956 earthquake and tsunami in Amorgos, Greece. Geophys. J. Int. 178 (3), 1533–1554.
Okal, E.A., Synolakis, C.E., 2004. Source discriminants for near-field tsunamis. Geophys. J. Int. 158 (3), 899–912.
Paris, R., Switzer, A.D., Belousova, M., Belousov, A., Ontowirjo, B., Whelley, P.L., Ulvrova, M., 2014. Volcanic tsunami: a review of source mechanisms, past events and hazards in Southeast Asia (Indonesia, Philippines, Papua New Guinea). Nat. Hazards 70 (1), 447–470.
Pelinovsky, E., Choi, B.H., Stromkov, A., Didenkulova, I., Kim, H.S., 2005. Analysis of tide-gauge records of the 1883 Krakatau tsunami. In: Satake, K. (Ed.), Tsunamis. Springer, Dordrecht, pp. 57–77.
Rabinovich, A.B., 1997. Spectral analysis of tsunami waves: separation of source and topography effects. J. Geophys. Res. 102 (C6), 12663–12676.
Rabinovich, A.B., Thomson, R.E., Stephenson, F.E., 2006. The Sumatra tsunami of 26 December 2004 as observed in the North Pacific and North Atlantic oceans. Surv. Geophys. 27 (6), 647–677.
Rabinovich, A.B., Lobkovsky, L.I., Fine, I.V., Thomson, R.E., Ivelskaya, T.N., Kulikov, E. A., 2008. Near-source observations and modeling of the Kuril islands tsunamis of 15 November 2006 and 13 January 2007. Adv. Geosci. 14, 105–116.
Rabinovich, A.B., 2010. Seiches and harbor oscillations. In: Handbook of Coastal and Ocean Engineering, pp. 193–236.
Sandanbata, O., Watada, S., Satake, K., Fukao, Y., Sugioka, H., Ito, A., Shiobara, H., 2018. Ray tracing for dispersive tsunamis and source amplitude estimation based on Green's law: application to the 2015 volcanic tsunami earthquake near Torishima, South of Japan. Pure Appl. Geophys. 175 (4), 1371–1385.

Sandanbata, O., Shiobara, H., Kusumoto, S., Kim, H.J., Oba, A., Liu, Q., Ueda, T., Ogawa, M., Takano, K., Kotobuki, I., Wang, Y., 2018. Technical Research Report, Earthquake Research Institute, the University of Tokyo. Equipment of Miniature instruments to measure tsunami waves in an experimental tank (in Japanese), 24, pp. 29–34. available at: http://www.eri.u-tokyo.ac.jp/GIHOU/archive/24_029-034.pdf.

Satake, K., Kanamori, H., 1991. Abnormal tsunamis caused by the June 13, 1984, Torishima, Japan, earthquake. J. Geophys. Res. 96 (B12), 19933–19939.

Satake, K., 2007. Volcanic origin of the 1741 Oshima-Oshima tsunami in the Japan sea. Earth Planets Space 59 (5), 381–390.

Sorensen, R.M., 2010. Basic Coastal Engineering, third ed. Springer Science & Business Media, p. 324.

Synolakis, C.E., Bardet, J.P., Borrero, J.C., Davies, H.L., Okal, E.A., Silver, E.A., Sweet, S., Tappin, D.R., 2002. April. The slump origin of the 1998 Papua New Guinea tsunami. Proc. R. Soc. Lond. A 458 (2020), 763–789.

Synolakis, C.E., 2003. Tsunami and seiche. In: Chen, W.F., Scawthorn, C. (Eds.), Earthquake Engineering Handbook. CRC Press, pp. 1–90 (Chapter 9).

Takagi, H., Pratama, M.B., Kurobe, S., Esteban, M., Aránguiz, R., Ke, B., 2019. Analysis of generation and arrival time of landslide tsunami to Palu City due to the 2018 Sulawesi earthquake. Landslides 16 (5), 983–991.

Tinti, S., Maramai, A., Armigliato, A., Graziani, L., Manucci, A., Pagnoni, G., Zaniboni, F., 2006. Observations of physical effects from tsunamis of December 30, 2002 at Stromboli volcano, southern Italy. Bull. Volcanol. 68 (5), 450–461.

Torrence, C., Compo, G., 1998. A practical guide to wavelet analysis. Bull. Am. Meteorol. Soc. 79, 61–78.

Walder, J.S., Watts, P., Sorensen, O.E., Janssen, K., 2003. Tsunamis generated by subaerial mass flows. J. Geophys. Res. 108 (B5).

Wang, X., Liu, P.L.-F., 2006. An analysis of 2004 Sumatra earthquake fault plane mechanisms and Indian Ocean tsunami. J. Hydraul. Res. 44, 147–154.

Watts, P., Grilli, S.T., Tappin, D., Fryer, G.J., 2005. Tsunami generation by submarine mass failure. II: predictive equations and case studies. J. Waterw. Port, Coast. Ocean Eng. 131 (6), 298–310.

Weatherall, P., Marks, K.M., Jakobsson, M., Schmitt, T., Tani, S., Arndt, J.E., Rovere, M., Chaye, D., Ferrini, V., Wigley, R., 2015. A new digital bathymetric model of the world's oceans. Earth Space Science 2, 331–345.

Wessel, P., Smith, W.H.F., 1998. New, improved version of generic mapping tools released. EOS Trans AGU 79 (47), 579.